Mon. Not. R. Astron. Soc. **313**, 1–7 (2000)

The triple-shell structure and collimated outflows of the planetary nebula NGC 6891

Martín A. Guerrero,[1,2] Luis F. Miranda,[3] Arturo Manchado[1,4] and Roberto Vázquez[3,5]

[1]*Instituto de Astrofísica de Canarias, Vía Láctea s/n, La Laguna 38200, Tenerife, Spain*
[2]*Department of Astronomy, University of Illinois at Urbana-Champaign, 1002 West Green Street, Urbana, IL 61801, USA*
[3]*Instituto de Astrofísica de Andalucía, CSIC, Apdo. Postal 3004, 18080 Granada, Spain*
[4]*Consejo Superior de Investigaciones Científicas, Spain*
[5]*Instituto de Astronomía, UNAM, Apdo. Postal 877, 22800 Ensenada, B.C., Mexico*

Accepted 1999 September 7. Received 1999 September 3; in original form 1999 May 17

ABSTRACT

Narrow-band Hα and [N II] images and high-dispersion spatially resolved echelle spectroscopy of the planetary nebula NGC 6891 are presented. These observations show a great wealth of structures. The bright central nebula is surrounded by an attached shell and a detached outer halo. Both the inner and intermediate shells can be described as ellipsoids with similar major to minor axial ratios, but different spatial orientations. The kinematical ages of the intermediate shell and halo are 4800 and 28 000 yr, respectively. The intershell time lapse is in good agreement with the evolutionary interpulse time lapse. A highly collimated outflow is observed to protrude from the tips of the major axis of the inner nebula and impact on the outer edge of the intermediate shell. Kinematics and excitation of this outflow provide conclusive evidence that it is deflected during the interaction with the outer edge of the intermediate shell. At the same time, both the kinematics and the morphology of the intermediate shell appear to be affected by this interaction.

Key words: stars: AGB and post-AGB – ISM: jets and outflows – ISM: kinematics and dynamics – planetary nebulae: individual: NGC 6891.

1 INTRODUCTION

NGC 6891 (PN G054.1–12.1) belongs to the very exclusive group of triple-shell planetary nebulae (PNe) (Chu, Jacoby & Arendt 1987; Chu et al. 1991). Its bright main nebula is surrounded by an attached shell and by an additional detached halo. Large faint haloes in PNe are most likely the result of mass loss on the asymptotic giant branch (AGB) during the thermal pulses of the helium-shell burning phase (TP-AGB). The properties of the central star of NGC 6891 are well known, as it has been the object of a detailed analysis using non-LTE models (Méndez et al. 1988). The atmospheric parameters of the central star ($T_{\rm eff} = 50,000$ K, $\log g = 3.9$), its mass ($0.75\,{\rm M}_{\odot}$) and evolutionary stage, as well as the distance to the nebula (3.8 kpc), are known to a high degree of reliability. Therefore, a kinematical study of NGC 6891 offers the rare opportunity of investigating in an individual PN the multiple-shell phenomenon in relation to the final phases in the evolution of its central star (Chu et al. 1991; Guerrero et al. 1996). Despite its brightness [$\log F({\rm H}\beta) = -10.65$, Webster 1983], a detailed morphological and kinematical study of the main nebula of NGC 6891 is not yet available.

Moreover, recent high-dispersion spectroscopy (Guerrero, Villaver & Manchado 1998) suggests the likely presence of a collimated outflow in NGC 6891. Collimated outflows are becoming a typical structural component in PNe (López 1997), although the mechanism for producing collimated outflows in PNe is currently an unresolved problem. The morphological and kinematical characterization of collimated outflows in PNe is of great importance as it is the first step to understanding the origin and formation mechanisms of such structures.

This paper presents high-dispersion spectroscopy and narrow-band imaging of NGC 6891 in the Hα and [N II] λ6583 emission lines. Special emphasis has been given to the description and analysis of the morphology and kinematics of the main nebula and attached shell, and to the investigation of the multiple-shell formation. The morphological and kinematical properties of the collimated outflow and its interplay with the main morphological components have also been investigated and reported.

2 OBSERVATIONS

Narrow-band CCD images of NGC 6891 in the Hα and [N II] λ6583 emission lines were obtained on 1997 July 25 on the 2.56-m Nordic Optical Telescope (NOT) at the Roque de los Muchachos Observatory (La Palma, Spain). The high-resolution adaptive camera (HiRAC) was used in combination with a thinned $2k \times 2k$ Loral chip, giving a plate scale of 0.11 arcsec pixel^{-1} and a field of view of 3.7 arcmin. The central wavelength and full

width at half-maximum (FWHM) of the filters are λ6563 and 9 Å in the Hα line, and λ6584 and 9 Å in the [N II] line. A 15-min exposure was secured for each filter. As deduced from stars in the field, the spatial resolution (FWHM) is 1.5 arcsec. The narrow-band images and the [N II] to Hα ratio map are shown in Fig. 1.

Long-slit echelle spectra of NGC 6891 were obtained with the Utrecht Echelle Spectrograph (UES) on the 4.2-m WHT at the Roque de los Muchachos Observatory on 1995 July 14 and with the IACUB spectrograph on the NOT telescope on 1997 July 27. The spectral resolution, spatial scale on the detector, and field of view on the sky were 6.5 km s^{-1}, 0.36 arcsec pixel^{-1}, and 160 arcsec, for the UES spectrum, and 9.5 km s^{-1}, 0.28 arcsec pixel^{-1}, and 60 arcsec, for the IACUB spectra. Three long-slit spectra were secured at different slit positions; the one along the major axis of the main nebula (PA 315°) was observed using UES (1100-s exposure time), whereas the spectra at PA 25° and 260° were collected using IACUB (1800-s exposure time). The slit positions are shown in Fig. 2.

3 RESULTS

3.1 Morphology

Fig. 1 shows the presence of the different shells and morphological components in NGC 6891. These are illustrated in Fig. 2 in order to provide an easy reference. The inner shell (the bright main nebula) is not only much brighter in the Hα image than in the [N II] one, but its morphology is also different. The Hα image shows a spindle-shaped morphology, 9 arcsec × 6 arcsec in size, with the major axis at PA 135° (Fig. 1, top-left panel). It appears almost rectangular at low intensities (see thick contour in Fig. 1, top-left panel). Two bright emission maxima can be distinguished in the Hα image along the minor axis (PA 19°) with a separation of 4 arcsec. It is noticeable that the brightness of the shell edge is point-symmetric, the S–SE and N–NW arcs being brighter. The morphology closely resembles that of the PN Cn 3 − 1 (Miranda et al. 1997). On the other hand, the [N II] image (Fig. 1, top-right

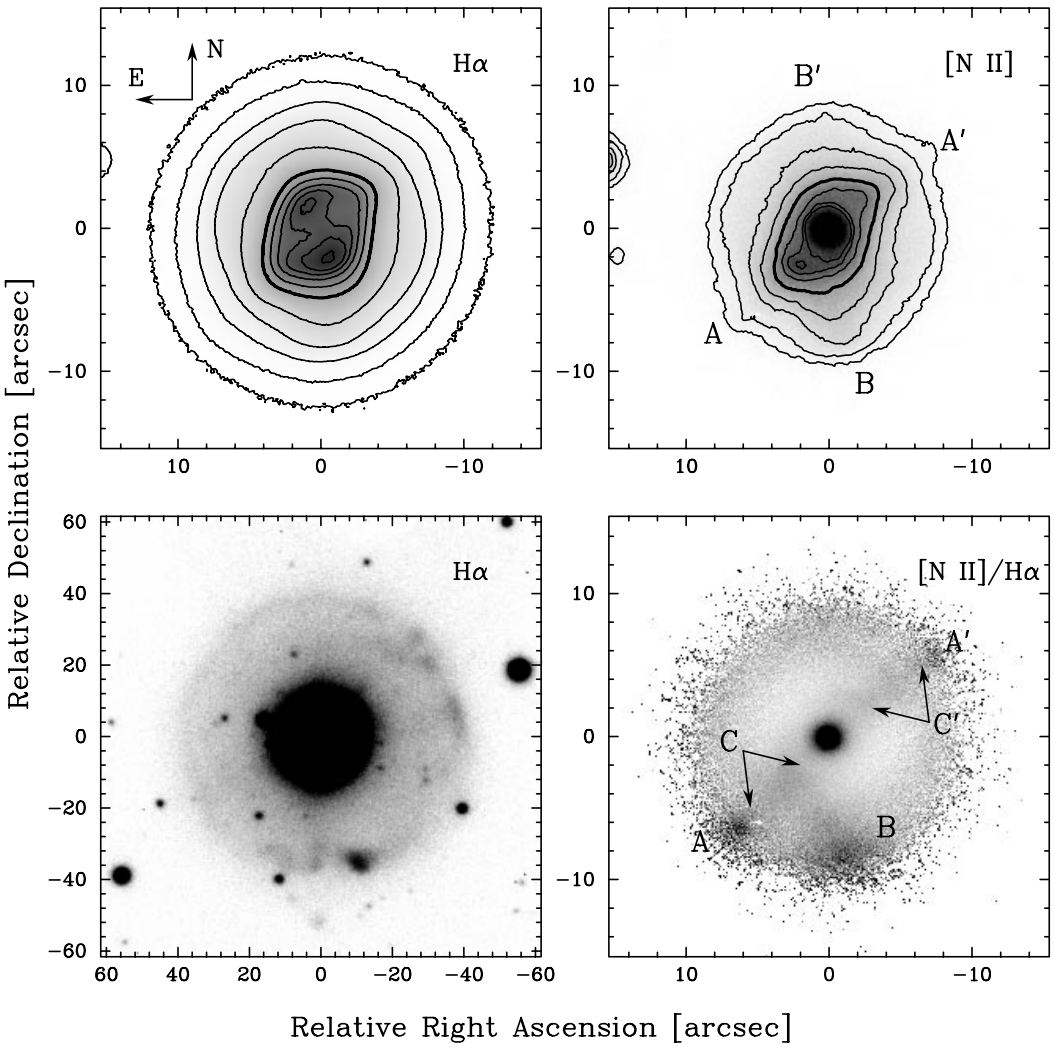

Figure 1. Negative grey-scale representation of CCD images of NGC 6891 in Hα (left column) and [N II] (top-right panel), and of the [N II] to Hα ratio map (lower-right panel). The grey-scale levels have been selected to emphasize the inner region an the intermediate shell (top row), and the halo in the Hα line (lower-left panel). The morphological features A–A′, B–B′ and C–C′ are labelled in the figure. Logarithmic contours have been overlaid over the *top* figures. The thick contour marks the outer limit of the inner shell.

panel) shows a remarkably S-shaped morphology. The S–SE and N–NW arcs described above in the Hα are enhanced in the low-ionization [N II] line. The strongest [N II] emission within these arcs is observed at the SE and NW tips of the major axis.

The intermediate shell is almost circular, with a diameter of 18 arcsec in the Hα image (Fig. 1, top-left). The surface brightness profile shows a linear decline as shown in Fig. 3, left panel. The [N II] image departs from the circular shape observed in Hα but does not follow a well-defined symmetry pattern. Two faint knots, A–A$'$, can be observed at PAs 135° and 315°, respectively. The [N II]/Hα ratio map (Fig. 1, lower-right panel) reveals two narrow stream-like structures, C–C$'$, which connect the major axis of the inner nebula to the A–A$'$ knots. The [N II] emission is also enhanced in two regions, B–B$'$, at PAs 188° and 8°, respectively, where the shell shape is swollen (see Fig. 1, top-right panel). The emission of these regions is more diffuse than in regions A–A$'$.

The outermost shell of NGC 6891 is a large (80 arcsec in diameter) faint halo detected in Hα (Fig. 1, lower-left panel), but not in the [N II] line (not shown here). The halo is also detected in the [O III] line (Manchado et al. 1996). High excitation is also observed in other haloes in PNe (Guerrero & Manchado 1999) and may be interpreted as an effect of the *hardening* of the radiation (Pottasch & Preite-Martinez 1983), indicating that the central regions of multiple-shell PNe (MSPNe) are optically thick to the ionizing radiation and that therefore only high-energy UV photons are able to reach the halo.

The halo is almost spherical, but appears slightly distorted towards the south where it seems to break and a peculiar spearhead-shaped outer structure can be seen. The Hα surface brightness declines steeply with radius as r^{-2} in the inner regions of the halo, but at $r = 23$ arcsec the fall stops and a smooth linear decline is observed, as shown in Fig. 3, right panel. The edge of this profile shows a small tip, between radii 34 arcsec and 40 arcsec, thus indicating a limb-brightened effect that has also been reported in other haloes of PNe (Chu et al. 1987; Balick et al. 1992). The profile then declines steeply at low intensities for radii up to 40 arcsec.

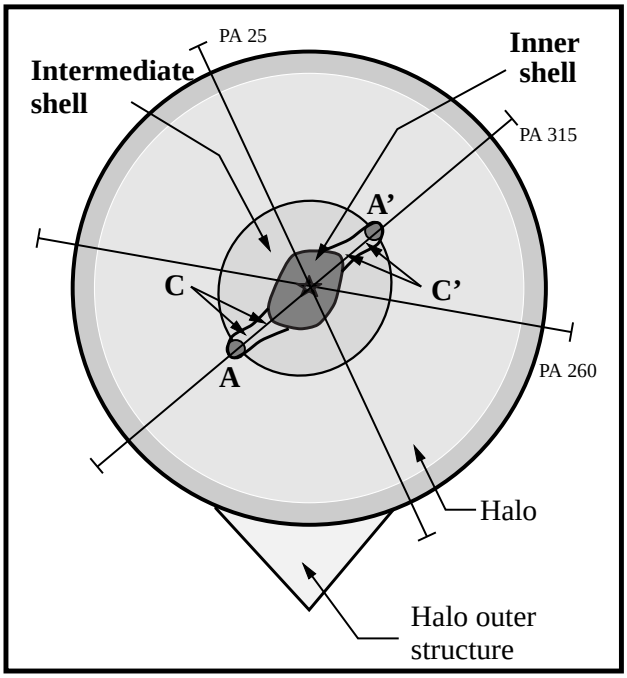

Figure 2. Sketch illustrating the main morphological features observed in NGC 6891 and the position of the slits.

3.2 Kinematics

Fig. 4 shows the long-slit echelle spectra of NGC 6891. The Hα line is shown only for the slit at PA 315°. The two emission maxima, located 3 arcsec from the centre, roughly correspond to those observed in the [N II] line. Since the line profile in the Hα line is broader than that in the [N II] λ6583 line, owing to its greater thermal broadening, the [N II] line will be used to describe the kinematics of NGC 6891.

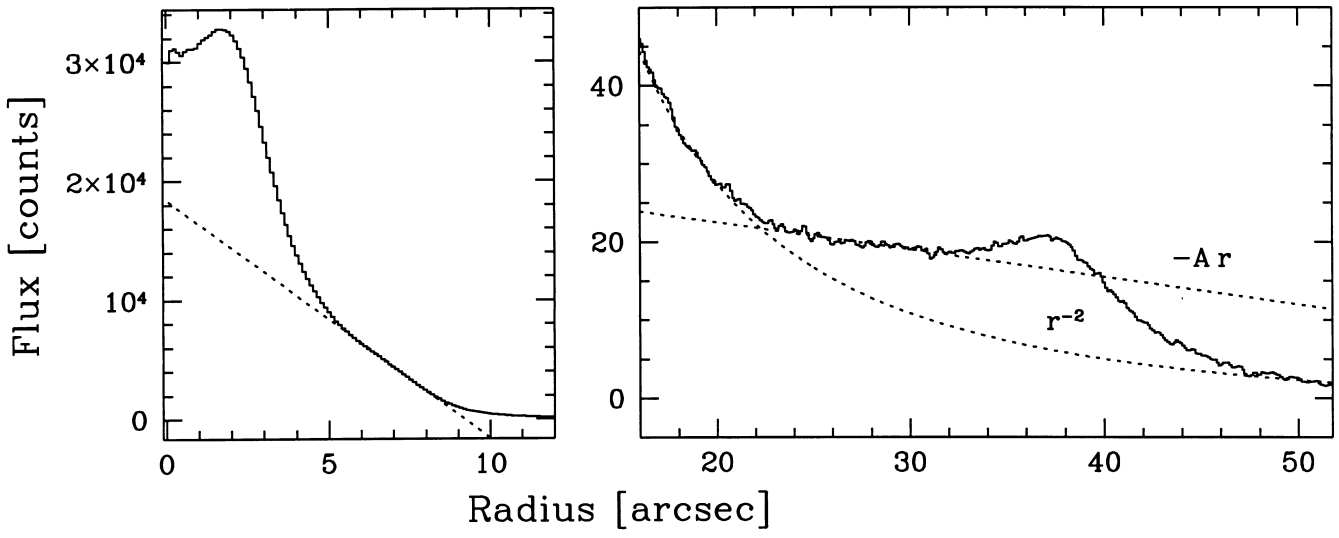

Figure 3. Hα surface brightness profile of the inner and intermediate shells (left) and halo (right) of NGC 6891. The inner and intermediate shells profile was extracted along the inner shell minor axis at PA 45°. The intermediate shell is well matched by a linear fit (dotted line). The halo profile was azimuthally averaged to increase the S/N ratio, excluding the southernmost part of the halo (from PA 165° to 205°) where it is not round. The inner region of the halo declines as r^{-2}, but the region between 23 and 34 arcsec is better described by a linear fit ($-A\,r$). Both fits are shown (dotted lines) in the figure.

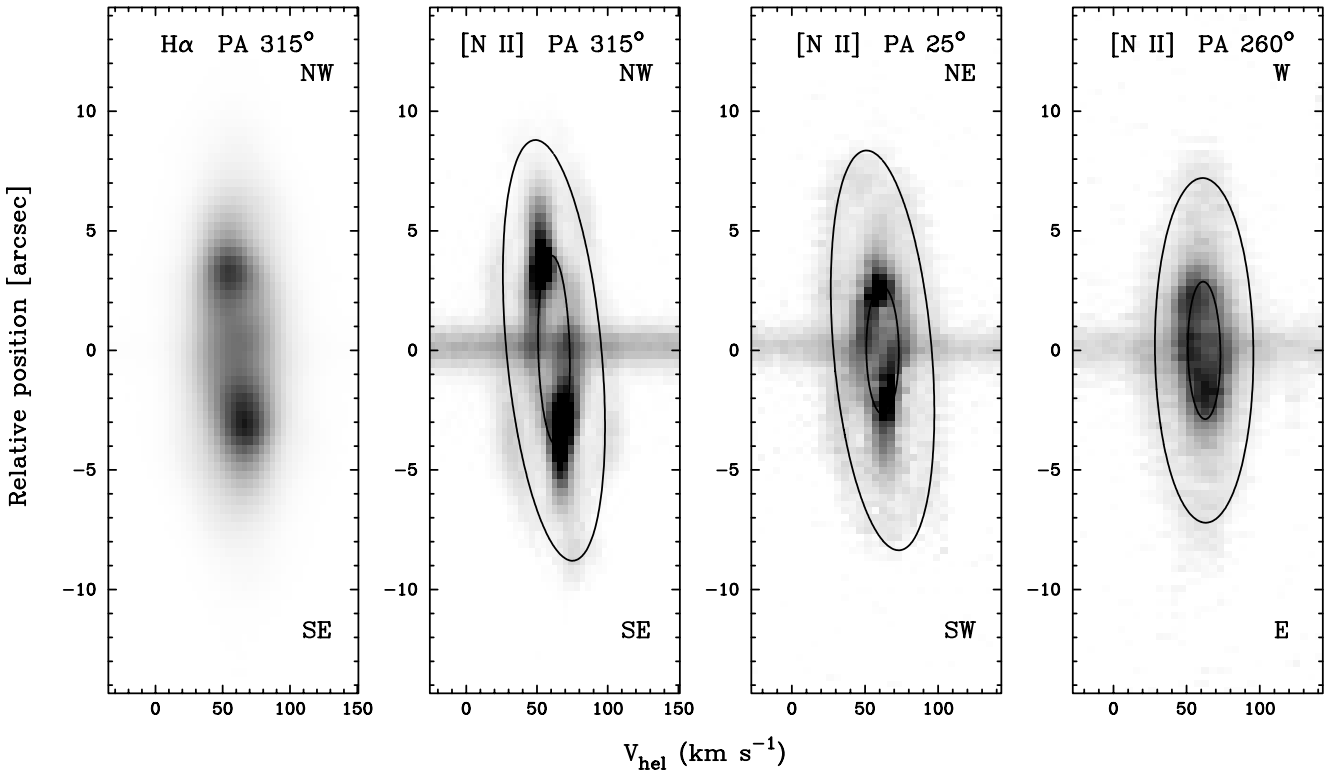

Figure 4. Negative grey-scale representation and contours of the Hα and [N II] emission-lines echellograms of NGC 6891 at PA 315°, 25° and 260°. The spatial orientation and scale and the velocity scale are given. The ellipse velocity predictions from the models described in the text for the inner and intermediate shells are shown.

The long-slit spectra of the inner shell at the different PAs show the typical line shape produced by an expanding shell. The line spliting is $19.1 \pm 0.3\,\mathrm{km\,s^{-1}}$ at the central position. As measured from the spectra, the shell size is smaller at PAs 25° and 260° (2.0–2.5 arcsec), close to its minor axis (PA 45°), than at PA 315° (the major axis). There is no significant ($\leq 2\,\mathrm{km\,s^{-1}}$) line tilt at PAs 25° and 260°, but this increases to $\sim 10\,\mathrm{km\,s^{-1}}$ at PA 315°. Both the morphological and kinematical properties of this shell may be described by a prolate shell whose approaching end of the major axis is tilted with respect to the line of sight along PA 315°. A simple ellipsoidal shell model with homologous expansion has been used to fit the kinematics of this shell. The results are overlaid in Fig. 4. The best fit is obtained for an inclination of 80°. The expansion velocity is $17\,\mathrm{km\,s^{-1}}$ and $10\,\mathrm{km\,s^{-1}}$ for the major and minor axes, respectively, and the semimajor axis is 3.8 arcsec.

The point-symmetry morphology of the inner shell is also recognized in the echellograms. The echellograms at PAs 25° and 315°, which are placed on the S–SE and N–NW brighter arcs, also show a point-symmetric brightness enhancement. The echellogram at PA 260°, however, does not show this enhancement because this echellogram does not cross the S–SE and N–NW arcs.

The line shape and brightness of the spectra at PAs 315° and 25° are dominated by two emission maxima at the edge of the inner shell that are also observed in the Hα line (see above). These features extend outwards and can be traced to 9 arcsec from the centre at PAs 135°–315°. Therefore, the ends of these features at PAs 135°–315° correspond to the knots A–A′. Their kinematical structure is better displayed in Fig. 5, which shows the [N II] to Hα emission-line ratio map at PA 315°. A narrow [N II]-emission-enhanced region (dark grey in Fig. 4) protrudes from the inner-shell edge and crosses the intermediate shell. It eventually goes beyond the outer edge of this shell. At this position, it increases its velocity by $7\,\mathrm{km\,s^{-1}}$ and the emission is enhanced in knots A–A′. The difference in velocity between each pair is only $12\,\mathrm{km\,s^{-1}}$ within the shell, and $28\,\mathrm{km\,s^{-1}}$ at the knots. The velocity width of these features, once deconvolved of instrumental effects and thermal broadening (assuming a T_e of 10^4 K), is very small, between 8 and $10\,\mathrm{km\,s^{-1}}$ within the intermediate shell, indicating that they are collimated outflows. They broaden up to 16–$20\,\mathrm{km\,s^{-1}}$ at the bright knots A–A′.

The long-slit spectra of the intermediate attached shell also show the typical emission-line pattern of an expanding shell. A line split of $59 \pm 1\,\mathrm{km\,s^{-1}}$ is measured at the stellar position. The emission line is tilted at PAs 25° and 315° but not at PA 260°. Interestingly, the inner-shell emission line at PA 25° does not show the tilt observed for the attached shell. This suggests that the symmetry axis of the intermediate shell does not coincide with that of the inner shell. To confirm this, a model of an expanding ellipsoid was also fitted to the data of the intermediate shell. The best fitting is shown in Fig. 4. The parameters of the fit are an inclination with the line of sight of 50°, an expansion velocity of $45 \pm 5\,\mathrm{km\,s^{-1}}$ at the poles and $28\,\mathrm{km\,s^{-1}}$ at the equator, a semimajor axis of 12.0 ± 1.5 arcsec and an orientation of the major axis at PA 160° ± 10°. The line shape is very regular at PAs 25° and 260°, which closely follow the simple ellipsoidal model used. Some small differences are noticeable between the proposed model and the kinematical data at PA 315°, providing evidence that the shell shape at this PA departs slightly from an ellipsoid. In addition, bright condensations are also found at the edge of the line at PA 315°. It is worth noting that they are present as pairs showing point symmetry.

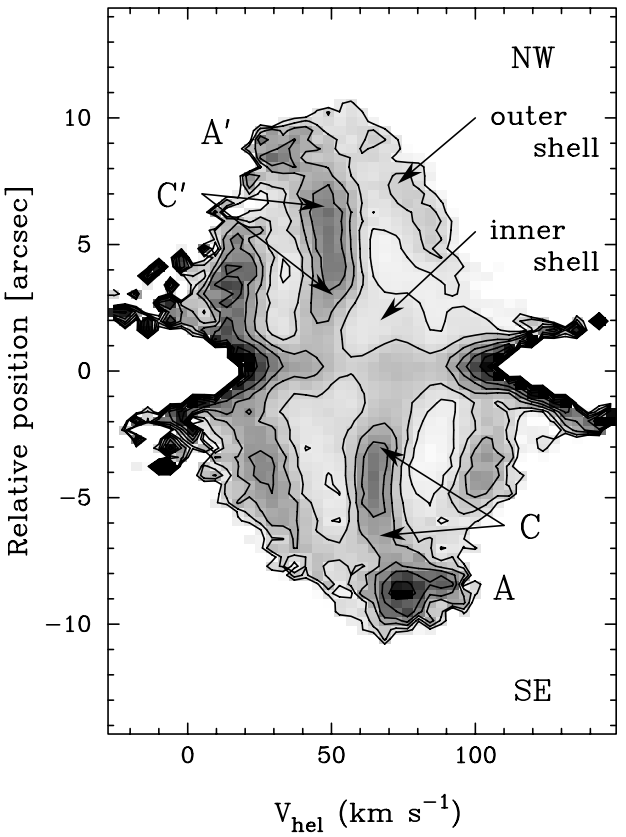

Figure 5. Negative grey-scale representation of the [N II] to Hα emission-line ratio map at PA 315°. The [N II]-enhanced emission regions are shown as dark grey. The different morphological features have been labelled. Note that a mask was applied to the stellar (ratio ~1) continuum.

4 DISCUSSION

4.1 The triple-shell structure

NGC 6891 is composed of three different shells. The bright central part is a prolate shell expanding at 10 km s^{-1} at its equator and 17 km s^{-1} at its tips. This shell is tilted 80° from the line of sight and oriented at PA 135°. The intermediate shell is expanding faster (28–45 km s^{-1}) than the inner shell into the outer halo. It exhibits the typical linear decline of the emission brightness profile of other PN attached shells (Frank, Balick & Riley 1990; Guerrero et al. 1998). The kinematics of this shell suggests that it can also be described by an ellipsoidal shell, expanding faster than the inner shell, in agreement with the predictions of the current hydrodynamical models (Mellema 1994; Steffen et al. 1997; Villaver et al. 1999). The intermediate shell is tilted 50° from the line of sight and is orientated at PA 160°, and therefore the symmetry axes of the inner and intermediate shells do not point in the same direction. The halo of NGC 6891 is a faint, almost circular detached shell, 1.5 pc in diameter. Its emission brightness falls steeply as r^{-2} until it stops, remains almost constant and rises up at the limb-brightened edge. Since a constant mass-loss rate would produce an r^{-3} emission brightness decline, the profile observed in the inner region of the halo reflects either a non-constant mass-loss rate during the late AGB evolution, or a redistribution of the material within the shell owing to dynamical effects, or both. The almost constant-brightness region and the tip at the edge of the halo strongly indicate that material is piled up at the outer region of the halo. However, at a height of 800 pc above the Galactic plane, the hypothesis that the interstellar medium (ISM) has significantly retarded the expansion of the leading edge of the halo seems implausible.

Given the distance, angular size and geometry, and expansion velocity of each shell in NGC 6891, the kinematical age may be worked out simply by dividing the nebular radius by the expansion velocity. Nevertheless, the velocity gradient of 20 km s^{-1} from the inner to the intermediate shell of NGC 6891 does not make the direct comparison between kinematical and evolutionary ages a straightforward task. Instead, the expansion velocity and size of the attached shell must be used as a reliable estimate of the PN age (Steffen et al. 1997). At a distance of 3.8 kpc (Méndez et al. 1988), the expansion velocity and geometrical parameters of the ellipsoidal-expanding shell fitted to the intermediate shell in Section 3.2 results in a kinematical age of 4800 yr. In contrast, the evolutionary age of the central star, which follows from the post-AGB evolutionary tracks of Vassiliadis & Wood (1994) for the central-star mass and effective temperature of NGC 6891 (Méndez et al. 1998), is too short (200 yr). This would indicate a transition time of 4600 yr.

According to the expansion velocity of the halo of 26 km s^{-1} reported by Guerrero et al. (1998), its kinematical age is 28 000 yr. The corresponding intershell time (the difference between the kinematical age of the halo and main nebula) is 23 000 yr. This value can be compared with the interpulse time, $\tau_{\rm IP}$, based on the idea that the haloes and shells of PNe are related to subsequent thermal pulses. The interpulse time can be evaluated using equation (4) from Vassiliadis & Wood (1994) for metallicity $Z = 0.008$ appropriate for high-latitude Galactic PNe,

$$\log \tau_{\rm IP} = 7.27 - 3.77\, M_{\rm c}, \qquad (1)$$

where $M_{\rm c}$ is the mass of the PN central star. For a core mass of 0.75 M$_\odot$ (Méndez et al. 1998), an interpulse time of 27 700 yr is obtained in good agreement with the kinematical intershell time.

4.2 The low-ionization collimated outflows

The high-collimation degree shown by the gas along C–C′ is quite noticeable; the measured FWHM of 10 km s^{-1} in the [N II] line yields a very small upper limit to the traversal motion of the gas into these stream-like structures. The maxima velocities along C–C′ are measured at the terminal knots A–A′, which show opposite systemic velocities of ±14 km s^{-1}. Since these velocities are projected on to the sky, the real expansion velocity must be faster. A lower limit is settled by the expansion velocity of the intermediate shell (45 km s^{-1}), as knots A–A′ are overtaking this shell. If we assume the inclination angle with the line of sight to be the same as the inclination of the inner shell (80°), a deprojected velocity of 80 km s^{-1} is calculated for knots A–A′. Therefore, C–C′ can be interpreted as fast collimated outflows, which originate at the inner-shell major-axis tips and traverse the intermediate shell.

Knots A–A′ show strong evidence of the interaction of the collimated outflow with the outer edge of the intermediate shell. The velocity increases, indicating that the outflow is accelerated or most probably deflected at the surface discontinuity between the intermediate shell and the halo. The FWHM also rises to 20 km s^{-1}, which indicates that traversal motions and turbulence increase in the outflow when it reaches the outer edge of the intermediate shell. All this indicates that a density enhancement is

found at the outer edge of this shell, or that the shell itself plays a significant role in the collimation of the outflow. In addition, the line shape at PA 315° does not exactly fit an expanding homologous ellipsoid; instead, emission is enhanced at different points in the position–velocity echellogram and the kinematics slightly depart from that expected for such a model. This is not likely to be fortuitous, but strengthens the idea that the interaction between the collimated outflow from inwards and the edge of this shell is taking place in this nebula.

Very similar phenomenology has also been described for NGC 6572 (Miranda et al. 1999b). In this case, kinematics and morphology provide conclusive evidence of a collimated outflow–shell interaction. As a result of this interaction, the shell has been broken up and presents peculiar kinematics. Collimated outflow–shell interaction can also be described in the case of IC 4593 (Corradi et al. 1997; O'Connor et al. 1999). A detailed inspection of the data by Corradi et al. shows that the behaviour of the collimated outflows at PAs 139° and 242° (knots A and C, respectively, as defined by Corradi et al.) is very similar to that described for NGC 6891. The outflows at PA 139° and 242° in IC 4593 are also sped up and the FWHM also increases as it reaches the shell edge at the position of IC 4593 knots A and C (see fig. 4 of Corradi et al. 1997). Interaction between collimated outflows and the nebula has been invoked by Sahai & Trauger (1998) to interpret multiple point-symmetric features observed at or near the border of the shell in several young PNe. All these data strongly suggest that interaction between collimated outflows and shells in PNe indeed occurs and may plays an important role in the shaping of the shell.

The knots A–A′, the collimated structures C–C′ and the regions B–B′ present a [N II]-to-Hα ratio enhancement indicative of the presence of low-ionization gas. Because they appear as pairs located on opposite sides of the central star, they may be considered as fast low-ionization emission regions (FLIERs), as they share many of the properties described in such structures (Balick et al. 1998, and references therein). Indeed, the morphology and kinematics of NGC 6891 share many similarities with other PNe that present FLIERs. In particular, there is a close resemblance to NGC 3242, 6826 and 7009, although it must be noted that the collimated outflow described in NGC 6891 is narrower than it is in NGC 7009. NGC 6751 (Chu et al. 1991) and IC 4593 (Corradi et al. 1997; O'Connor et al. 1999) are also very similar objects. All of them show the same structure: an elliptical or prolate inner shell, a round attached intermediate shell and a detached halo (Chu et al. 1987; Bässgen & Grewing 1989), and a fast outflow of low-ionization material is observed at or near the tip of the major axis of the inner shell (Balick et al. 1998).

There is growing evidence for a close relation between FLIERs, collimated outflows and ansae, and the inner shells (NGC 3242, 6751, 6826 and 7009) or inner structures (IC 4593) of multiple-shell PNe. It is interesting to note that the lowest-ionization regions are found in all cases at the outer edge of the intermediate shell. These elements seem to be of physical importance in the collimation of an outflow within the attached outer shell. But a new element is added in NGC 6891: the point-symmetric distribution of the brightness of the inner shell, both in the morphology and kinematics, may be related to the physical conditions required to the collimating mechanism.

The formation mechanisms of such structures in PNe are still unknown. Only under unrealistic conditions for the mass-loss rate (Borkowski, Blondin & Harrington 1997) or restrictive conditions for the fast wind velocity (Frank, Balick & Livio 1996) the proposed models can reproduce collimated outflows along the major nebular axis (but see Dwarkadas & Balick 1998). The situation turns out to be even worse because more exotic phenomena, invoking the precession or rotation of the collimating agent, are being observed in an increasing number of PNe. The precessing bipolar collimated outflows reported for NGC 6543 (Miranda & Solf 1992) and NGC 6884 (Miranda, Guerrero & Torrelles 1999a), the kinematical properties of point-symmetric PNe (Guerrero, Vázquez & López 1999), or the bipolar rotating episodic jets (BRETs) (López, Meaburn & Palmer 1993; Bryce et al. 1997) increase the difficulties of the interpretation. In such cases, the explanation invokes the presence of a close binary companion for the central star of the PN going through a common envelope phase, or magnetic fields, or both (see Livio & Pringle 1997, and references therein; García-Segura 1997).

The great wealth of structures within NGC 6891 will obviously benefit from high-resolution narrow-band images in low-ionization species. In particular, these would help to reveal the detailed geometry between the inner shell and the collimated outflows C–C′, as well as to confirm whether the point symmetry of this shell is connected to the collimation mechanism. In addition, intermediate-dispersion spectroscopy of the low-ionization emission regions will be very valuable for working out the physical conditions and chemical abundances in these regions and comparing them with other FLIERs.

5 SUMMARY AND CONCLUSIONS

We summarize our results and conclusions below.

(i) The nebular structure of NGC 6891 reflects the different mass-loss episodes experienced by its progenitor star on the tip of the AGB phase and on the post-AGB stage. The halo was formed some 28 000 years ago during the mass-loss episode associated with a period between thermal pulses on the late AGB phase. Some 4800 years ago, the progenitor star ejected most of its remaining envelope, and the intermediate and inner shells arose.

(ii) The previous interpretation is in good agreement with the current AGB intershell time-lapse predictions, although a significant transition time (4600 yr) must be allowed.

(iii) The inner and intermediate shells may be described by a simple model of an expanding ellipsoid. Expansion velocities of 17 and 10 km s^{-1} for the inner shell, and 45 and 28 km s^{-1} for the intermediate shell are worked out. Although the major-to-minor-axis ratio is almost the same for both shells, the spatial orientation of the shells is different.

(iv) A fast collimated outflow ($v_{\rm exp} > 45$ km s^{-1}) runs from the tips of the major axis of the inner shell throughout the intermediate shell until it reaches the outer edge of this region. This is interpreted as a FLIER.

(v) The kinematics and excitation of knots A–A′ provide conclusive evidence of the interaction between the collimated outflow and the outer edge of the intermediate shell. The outflow is deflected during the interaction, while the outer edge of the intermediate shell departs from an elliptical shape.

ACKNOWLEDGMENTS

The William Herschel Telescope and Nordic Optical Telescope are operated on the island of La Palma in the Spanish Observatorio del Roque de los Muchachos of the Instituto de Astrofísica de Canarias by the Royal Greenwich Observatory and Lund

Observatory, respectively. MAG and AM are partially supported by Spanish grants PB94–1108 and PB97–1435–C02–01. MAG is also supported partially by the Dirección General de Enseñanza Superior e Investigación Científica of Spanish Ministerio de Educación y Cultura. LFM and RV are partially supported by Spanish grant PB95–0066 and Junta de Andalucía. RV also acknowledges a graduate scholarship from AECI (Spain) and complementary support from DGAPA–UNAM (Mexico).

REFERENCES

Balick B., Gonzalez G., Frank A., Jacoby G., 1992, ApJ, 392, 582
Balick B., Alexander J., Hajian A. R., Terzian Y., Perinotto M., Patriarchi P., 1998, AJ, 116, 360
Bässgen M., Grewing M., 1989, A&A, 218, 273
Borkowski K. J., Blondin J. M., Harrington J. P., 1997, ApJ, 482, L97
Bryce M., López J. A., Holloway A. J., Meaburn J., 1997, ApJ, 487, L161
Chu Y.-H., Jacoby G. H., Arendt R., 1987, ApJS, 64, 529
Chu Y.-H., Manchado A., Jacoby G. H., Kwitter K. B., 1991, ApJ, 376, 150
Corradi R. L. M., Guerrero M. A., Manchado A., Mampaso A., 1997, New Astron., 2, 461
Dwarkadas V., Balick B., 1998, ApJ, 497, 267
Frank A., Balick B., Riley J., 1990, AJ, 100, 1903
Frank A., Balick B., Livio M., 1996, ApJ, 471, L53
García-Segura G., 1997, ApJ, 489, L189
Guerrero M. A., Manchado A., 1999, ApJ, 522, 378
Guerrero M. A., Manchado A., Stanghellini L., Herrero A., 1996, ApJ, 464, 847
Guerrero M. A., Villaver E., Manchado A., 1998, ApJ, 507, 889
Guerrero M. A., Vázquez R., López J. A., 1999, AJ, 117, 967
Livio M., Pringle J. E., 1997, ApJ, 486, 835
López J. A., 1997, in Habing H. J., Lamers H. J. G. L. M., eds, Proc. IAU Symp. 180, Planetary Nebulae. Kluwer, Dordrecht, p. 197
López J. A., Meaburn J., Palmer J. W., 1993, ApJ, 415, L135
Manchado A., Guerrero M. A., Stanghellini L., Serra-Ricart M., 1996, The IAC Morphological Catalog of Northern Galactic Planetary Nebulae. IAC Publishing, La Laguna, Tenerife, Spain
Mellema G., 1994, A&A, 290, 915
Méndez R., Kudritzki R. P., Herrero A., Husfeld D., Groth H. G., 1988, A&A, 190, 113
Miranda L. F., Solf J., 1992, A&A, 260, 397
Miranda L. F., Vázquez R., Torrelles J. M., Eiroa C., López J. A., 1997, MNRAS, 288, 777
Miranda L. F., Guerrero M. A., Torrelles J. M., 1999a, AJ, 117, 1421
Miranda L. F., Vázquez R., Corradi R. L. M., Guerrero M. A., López J. A., Torrelles J. M., 1999b, ApJ, 520, 714
O'Connor J. A., Meaburn J., López J. A., Redman M. P., 1999, A&A, 346, 237
Pottasch S. R., Preite-Martinez A., 1983, A&A, 126, 31
Sahai R., Trauger J. T., 1998, AJ, 116, 1357
Steffen M., Schönberner D., Kifonidis K., Stahlberg J., 1997, in Habing H. J., Lamers H. J. G. L. M., eds, Proc. IAU Symp. 180, Planetary Nebulae. Kluwer, Dordrecht, p. 368
Vassiliadis E., Wood P. R., 1994, ApJS, 92, 125
Villaver E., Manchado A., García-Segura G., Guerrero M. A., 1999, Proc. IAU Symp. 191, AGB stars. Kluwer, Dordrecht, in press
Webster B. L., 1983, PASP, 95, 610